Physicochem. Probl. Miner. Process., 56(4), 2020, 625-640

http://www.journalssystem.com/ppmp

Physicochemical Problems of Mineral Processing

ISSN 1643-1049

Received March 06, 2020; reviewed; accepted June 03, 2020

Pourbaix diagrams for copper ores processing with seawater

Oscar A. Marín [1], Javier I. Ordóñez [1], Edelmira D. Gálvez [2], Luis A. Cisternas [1]

[1] Departamento de Ingeniería Química y Procesos de Minerales, Universidad de Antofagasta, 1240000 Antofagasta, Chile

[2] Departamento de Ingeniería Metalúrgica y Minas, Universidad Católica del Norte, 1240000 Antofagasta, Chile

Corresponding author: luis.cisternas@uantof.cl (Luis Cisternas)

Abstract: Decreases in the copper grade, waste disposal, energy supply, and water scarcity are some of the most critical challenges for the copper mining industries. One of the alternatives to counteract the water scarcity is the use of seawater, whether raw, partially desalinated, or desalinated. The use of seawater implies the generation of several compounds as a result of the interaction of ions in waters and ores. For this reason, it is required a greater understanding of these compounds generated on mineral processing, being Pourbaix diagrams used to estimate the possible compounds that will be formed in an aqueous medium for a given metal ore. In this paper, the effect of temperature, salinity, and Cu-concentration on the stability of the copper-solid species was investigated by constructing Pourbaix diagrams for different copper ore types with seawater. The results show that the corrosion areas decrease when the temperature increases for both oxidized and sulfide minerals. It was confirmed that the concentration is a critical variable that influences the size of corrosion areas. In terms of the effect of the other ions that seawater contains, carbonate, chloride, and bromide affect the stability of the Cu-solid species. The proposed diagrams serve as a useful tool to predict the stable species that may be obtained when seawater is used. The use of seawater in mining is an essential issue because it is considered as a more sustainable alternative instead of use freshwater or desalinated seawater, especially in locations with complex water availability, as is northern Chile.

Keywords: Pourbaix diagrams, Eh-pH diagrams, seawater, copper minerals, Chilean mining

1. Introduction

In Chile, mining is one of the main economic activities, reaching 10.1% of the GDP in 2018 (COCHILCO, 2019). Chile reserves are varied, including copper, gold, silver, molybdenum, nitrates, lithium, potassium, iodine, among other deposits. Its reserves can vary from 6.7% of the world's gold, 27.7% of copper, and 100% of natural nitrates (Cisternas and Gálvez, 2014). All this large-scale production faces significant challenges, within which highlight energy supply, water scarcity, waste disposal, and the decline in the ore grades. Thus, for copper mining industries, including the total of mining operations, i.e., hydrometallurgical and concentration paths, the copper ore grade declines in 51% between 2001 and 2015 (Lagos et al., 2018). For this reason, to compensate for the decreasing grades, larger quantities of ore must be processed to accomplish production goals; as a result, the consumption of water and energy increases, as well as mining wastes and greenhouse gas (GHG) emissions. This situation will increase in the future since the ore copper grades are expected to continue to decline, which will imply significant upward pressure on the GHG, energy, and water intensity of copper production (Northey et al., 2013). Therefore, the mining activity is projected to develop these challenges not only from an economic and technical perspective but also from incorporating the focus environmental and social, under the global sustainable development perspectives (Ali et al., 2018).

In the sustainability context, is that the water supply has become critical, mainly due to its demand and scarcity. Of all the water available on the planet, the freshwater only represents about 2.5%, 1.9% of this resource is on polar ice caps and glaciers, 0.6% is groundwater, and about 0.01% is on the surface (Cavin, 2017). Also, climate change, economic development, and population growth will affect the total

DOI: 10.37190/ppmp/123407

water availability in the world. In a study accomplished by Luo et al. (2015), several countries are analyzed according to demands and supply projections estimating the water stress for specific periods. There are countries as Estonia, Namibia, and Chile, among others, which could face a significant effect on water stress from 2010 to 2040. Specifically, Chile would increase its water stress index by 53%. Water scarcity is and will be one of the main issues for countries, extending even beyond the national boundaries (Hoekstra and Chapagain, 2008). Although mining operations are considered a low water consumer operation, they can locally affect the natural flows and the quality of the natural resources (Northey et al., 2016). For example, in the Antofagasta region (Chile), mining operations consume between 60-70% of the water resources. For Chilean mining, these problems are even worsened, due most of the mining deposits are located in desert areas and high altitudes. The more valuable copper mines are situated in the Atacama Desert, the aridest area on earth (Clarke et al., 2006), and at altitudes that vary between 600 and 3,000 meters above sea level. The desert and the high altitude makes access to any water source even more complicated.

1.1. Mining and seawater

For mining processes, one of the alternatives to counteract the water scarcity is the use of raw, partially desalinated or desalinated seawater (Cruz et al., 2019). Particularly in Chile, from 2010 to 2015, the use of seawater with or without desalination increased more than ten times. Currently, seven mining companies are using raw seawater in their processes, while there are ten desalination plants and eleven new projects for the operation of new desalination plants (Gálvez and Cisternas, 2017; Herrera-León et al., 2019). These plants operate through reverse osmosis (RO), which is the most used technology worldwide to desalinate seawater and brackish water, mainly due to its capability to treat large volumes. Examples of RO plants in mine operations are Pampa Camarones Mining, BHP Billiton, Tocopilla Mining Company, and Antofagasta Minerals Group in Centinela Mining. The seawater consumption by Chilean copper mining is 23% (COCHILCO, 2019); it is expected to 2027, an increase up to 46% respect to the total water requirement. According to COCHILCO (2019), the higher water consumption in the copper industry is in the concentrator plant with over 60% of the total, while the hydrometallurgy process (leaching) consumes only the 13% of the total. Chile and Peru, the two largest copper-producing countries, will see an increase in water supply from desalination projects (Dixon, 2013).

Despite the RO provides water with high quality that generally does not affect the mineral processing, it involves two main environmental drawbacks: i) a discharged brine with a salinity twice seawater is released to the ocean, together with chemical reagents such as antiscalants, coagulants and cleaning additives, which may cause adverse environmental effects (Elimelech and Phillip, 2011; Ordóñez et al., 2015) and ii) reverse osmosis is an energy-intensive process, which is commonly associated with fossil-based power generation that generates greenhouse gas emissions (Cruz et al., 2019).

In this sense, there are several studies about the use of raw seawater directly in the mining processes. The effect of seawater on flotation has been studied for several research groups and reviewed by several authors (Castro, 2018; Jeldres et al., 2016; Suyantara et al., 2018; Wang and Peng, 2014). The seawater affects different phenomena such as bubble stability and pulp rheology. The effect of seawater ions and their aqua-complexes can impact positively and negatively depending on the mineral studied, operational conditions, and objectives searched. For example, the presence of copper ions can activate sphalerite and pyrite (Mu and Peng, 2019; Wang et al., 2019). Positive, negative, and uncharged copper species interact with mineral surfaces affecting its floatability. Wang et al. (2019) found that the adsorption and precipitation of hydrolyzed copper ions result in sphalerite activation. In another study, it was discovered that seawater significantly increases pyrite recovery in flotation when chalcopyrite is also present (Mu and Peng, 2019). This was explained by the increased copper activation on the pyrite surface because chalcopyrite is more electrochemically active with more substantial oxidation in seawater than in freshwater. Therefore, the understanding of the stability species of copper in seawater is essential.

Regarding hydrometallurgical processes, seawater is used in leaching due to the high concentration of chloride that acts as an oxidizing agent (Torres et al., 2015). Watling (2014) made a review of the acidic chloride leaching options and resumed their advantages as (i) increased solubility of iron and other metals; (ii) better redox properties due to the stabilization of the Cu(I)/Cu(II) redox couple as chloride complexes; (iii) faster leaching kinetics; (iv) better diffusion due to the formation of porous elemental sulfur; and (v) low pyrite reactivity. Some of their disadvantages are: (i) the corrosive effect of chloride; (ii) the diminution of the particle size in atmospheric temperature-pressure operation; and (iii) the difficulties in the electro-winning plant. Also, increased total dissolved solids, viscosity, and density of the process water produce increased amounts of secondary precipitates that may trek through the bed, block solution channels, and reduce permeability in the heap leaching stage (Miller, 1998). Several studies have shown that leaching using seawater can produce better recoveries (Hernández et al., 2018, 2015).

Seawater contains chemical elements and compounds such as sodium, magnesium, potassium, calcium as cations and chloride, carbonate, sulfate, and bicarbonate as anions, among others. Some elements are challenging to quantify because they appear in extremely low concentrations, and usually average data are given. The total of compounds reaches 3.5%, and the rest 96.5% is pure water. This composition varies from one place to another, but the relative composition is considered constant (Cisternas and Gálvez, 2017). Depending on the local evaporation, the salinity varies from 30 to 40 g/L. The seawater also contains gases such as nitrogen, carbon dioxide, and oxygen (Valderrama et al., 2017). The dissolved oxygen determines the oxidation/reduction behavior of the seawater, the dissolved CO_2 (or H_2CO_3) produces seawater to become acidic. At the same time, $B(OH)_3/B(OH)_4^-$ and HCO_3^-/CO_3^{2-} ions are responsible for their basic behavior, being the HCO_3^- molarity concentration in seawater close to 2.8 times more than in freshwater, being the natural pH of seawater around 7.8-8.2 (Castro, 2018). The amount of H_2CO_3 at the natural pH of seawater is significantly low compared to ions HCO_3^-/CO_3^{2-}.

The presence of these elements affects the physical and chemical properties of the seawater. Salinity and temperature are the two most important variables that determine the properties of seawater. For example, density and viscosity increase with salinity and may intervene in the fluid-transport in plants. Other properties as vapor pressure and surface tension are related to water evaporation and interaction with solid particles, respectively, and can affect, for example, the leaching process. This variability can impact positively or negatively the mining operations.

On the other hand, the determination of the characteristics of seawater is given by the chemical speciation, which implies that an element can be present in different chemical forms depending on the solution conditions. The speciation of seawater compounds depends strongly on pH. In the case of trace metals present in the seawater, they can be classified by the inorganic ligands that complex them into five groups (hydrolyzed, carbonate, chloride, free, and transition metals) (Byrne et al., 1988). Within the number of elemental forms hydrolyzed in seawater, i.e., metals involved in the chlorine complexation, Cu(I), Ag(I) and Au(I), are slightly pH-dependent (Byrne, 2002). The same occurs with metals in the free form, except Iron (II) and Nickel (II) that form carbonate complexes. Metals that complexes strongly with hydroxides a decrease in pH will no change their free form, only the amount of hydroxides per metal (e.g., from $Al(OH)_4^+$ to $Al(OH)_3$). The metals that complexes with carbonate as Cu(II), UO_2(II), and rare earth are strongly affected by pH, increasing in their free form (Millero et al., 2009).

1.2. Pourbaix diagrams

Pourbaix diagrams, which are also called Eh-pH diagrams, were developed by Marcel Pourbaix in his Ph.D. thesis. He is the author of the well-known Pourbaix diagram handbook, where an extensive collection of diagrams for various aqueous systems can be found (Pourbaix, 1966). The Pourbaix diagrams are employed in almost any area associated with aqueous chemistry due to take into account chemical and electrochemical stability for different redox states of a particular element at specific potential (ESHE) and pH (Haung, 2016). In an aqueous mixture at fixed Eh-pH-condition, a large number of different species exist simultaneously. The Pourbaix diagrams simplify the analysis by showing only the predominant species in each stability area. Besides, lines represent the Eh-pH-conditions where the adjacent species are in the equilibrium state (Kobylin et al., 2014). For this reason, it is said that Pourbaix diagrams define the stability domain of electrolyte, metal, and related

compounds (e.g., oxides, hydroxides, and hydrides). Complexing agents, such as ammonia, bromides, carbonates, chlorides, cyanides, and sulfates, can alter visibly the areas of the diagrams, product of the formation of highly stable complexes in solution.

The use of the Pourbaix diagram has many applications, such as coating, electric cells, industrial electrolysis, and water treatment. One of its primary functions is in the corrosion area, being useful for the estimation of corrosion products at different pH, potential combinations, and the conditions to reduce or prevent corrosion (Belmonte et al., 2015; Su et al., 2016). Also, it has been used in fields as varied as are nanotechnology or geology. Dezfoolian et al. (2015) used the Pourbaix diagrams of copper and zinc in aqueous electrolytes to predict the possible species formed when they synthesized simultaneously copper and zinc oxides nanostructures by anodization of brass foil in alkaline aqueous solution at room temperature. Yagi et al. (2009) synthesized Cu and Cu_2O nanoparticles selectively by chemical reduction from CuO aqueous suspension. They demonstrated that the most stable chemical species could be determined by comparing the mixed potential with the information from the Pourbaix diagrams, where the kind of species synthesized can be controlled by the mixed potential, which is altered by pH and temperature, both easily controllable. In the case of geology, it is having been widely used to explain the geological processes associated with fluids. Yang et al. (2014) constructed the Pourbaix diagram for the Si-Fe-Mn-H_2O system at 300 °C for hydrothermal fluid and at 25°C for seawater, to decipher precipitation conditions at the Pacmanus hydrothermal field. Through the integration of the Eh-pH diagrams, they were able to explain the formation of Si-Fe-Mn solid species when hydrothermal fluid is mixed with seawater at different conditions of pH and temperature. Pourbaix diagrams have applications to flotation systems; for example, they have been used to study the enargite depression in seawater (Yepsen et al., 2019).

Pourbaix diagrams have also been applied in hydrometallurgical processes. von Bonsdorff et al. (2005) studied the application of different electrodes for the measurement of the potential analyzing the stability of copper ions in the HydroCopper process, in which the chalcopyrite ore ($CuFeS_2$) is processed using a chloride base without the addition of acid or base reagents. Fan et al. (2013) proposed an alkaline leaching process with NaOH to separate tellurium and selenium selectively from a high tellurium bearing material. They constructed the Pourbaix diagram for the Cu-Te-Se-H_2O system to compare thermodynamic calculation data with experimental results, and they concluded that the experimental results with calculation data agreed reasonably well. There are several applications in leaching studies; for example, the potential-pH diagram of the Pb/Ag/Bi-H_2O system was used to assess the possibilities of the selective leaching of lead and silver (Xing et al., 2019). In another example, Watling (2014) studied the leaching of a low-grade copper sulfide ore in three media, freshwater, seawater, double-strength seawater. They constructed diagrams for copper, iron, and aluminum to predict the possible compounds formed for the start and end of the 28 days of leaching. Some of its conclusions were that the use of saline water in the heap leaching could result in lower extraction efficiency, channeling, and reducing heap permeability, due to the increase in the formation of secondary precipitates.

It is essential to consider all the positive and negative effects of using seawater on mineral processing. For this, we can predict the possible compounds to be formed for a given metal in an aqueous medium, this being possible using the Pourbaix diagrams. In the literature exists many Pourbaix diagrams for different metals in freshwater. Still, it is rare to find these diagrams for the same metals in seawater, with which the present study seeks to contribute to this lack of information with the proposal of a methodology to generate the Pourbaix diagrams for metallic species in seawater.

This study aims to analyze the effect of seawater with four different salinity levels on the stability of several copper-solid species. The proposed methodology was used for the construction of the Pourbaix diagrams for the Covelline (CuS), Chalcocite (Cu_2S), Tenorite (CuO), Cuprite (Cu_2O), Chalcopyrite ($CuFeS_2$), and Bornite (Cu_5FeS_4) copper-solid species. Once these diagrams were constructed, the formation of passivation and corrosion areas were analyzed, and their effects in the leaching operation discussed.

2. Materials and methods

The Pourbaix diagrams were developed using HSC Enthalpy–entropy and heat capacity software and database (HSC chemistry model, v.9). This software utilizes the Stability Calculations for Aqueous

Systems (STABCAL) module (Haung, 1989; Haung and Cuentas, 1989). Four different kinds of waters were simulated, which were increasing their salinity level (‰), to analyze the effect of these aqueous solutions on the stability of several copper-solid species. Starting from 0‰ for pure water, 35‰ for seawater, 50‰ for brackish water and ending with 70‰ for brine. For this, we use the reference composition of seawater (Millero et al., 2008), see Table 1. It is important to note that although the salinity depends on the geographical location, the relative proportion of major ions, such as Na/CI, K/Cl, Mg/Cl, and Br/CI ratios, remain constant (Millero, 1974; Wright and Colling, 1995). For this reason, the chosen composition of seawater is suitable for the study on the effect of the salinity level on copper speciation.

The simulated brackish water can be approached operationally as a process water obtained by recirculation, where the salts are concentrated and seawater is used as 'make-up' water. On the other hand, the brine (or hypersaline water) is produced as a discharge from the desalination process by reverse osmosis, where the production of a water without salts implies the generation of another stream with a double concentrated solution (Loizides, 2000). The use of this type of solution has been experimentally observed recently for the hydrometallurgical processing of caliche and copper sulfide and concentrate ores, opening an opportunity to avoid its discharge into the ocean (Ordóñez et al., 2015; Velásquez-Yévenes and Quezada-Reyes, 2018). The composition of brackish water and brine, as well as the ionic strengths, were calculated, the latter by using Equation (1).

$$I = \frac{1}{2} m \sum X_i Z_i^2 \tag{1}$$

Where m is the molal concentration (mol of solute/kg of solvent), which can be calculated by Equation (2).

$$m = \frac{1}{A} \frac{S_R}{1 - S_R} \tag{2}$$

Table 1. Reference Composition of seawater (modified from Millero et al., 2008)

Solute i	Mole fraction, $10^7 X_i$	Atomic weight by molar fraction, $X_i A_i$ (g/mol)	Mass fraction, w_i (g/kg)	Concentration, x_i (mol/kg)	Charge of solute i, Z_i
Na^+	4188071	9.6282786	10.78145	0.46897	+1
Mg^{2+}	471678	1.1464134	1.28372	0.05282	+2
Ca^{2+}	91823	0.3680082	0.41208	0.01028	+2
K^+	91159	0.3564162	0.39910	0.01021	+1
Sr^{+2}	810	0.0070972	0.00795	0.00009	+2
Cl^-	4874839	17.2827667	19.35271	0.54587	-1
SO_4^{2-}	252152	2.4222377	2.71235	0.02824	-2
HCO_3^-	15340	0.0935998	0.10481	0.00172	-1
Br^-	7520	0.0600878	0.06728	0.00084	-1
CO_3^{2-}	2134	0.0128059	0.01434	0.00024	-2
$B(OH)_4^-$	900	0.0070956	0.00795	0.00010	-1
F^-	610	0.0011589	0.00130	0.00007	-1
OH^-	71	0.0001208	0.00014	0.00001	-1
$B(OH)_3$	2807	0.0173565	0.01944	0.00031	0
CO_2	86	0.0003785	0.00042	0.00001	0
Sum	10000000	31.4038218	35.16504	1.11977	-

where $A = \sum X_i A_i$ is the mole-weighted average atomic weight of the element in sea salt 31.4038218 g/mol, S_R is the reference composition salinity, and S is the practical salinity. For pure water, S_R is defined to be zero, while for seawater, it is defined to be exactly 35.16504 g/kg (Millero et al., 2008). S_R in terms of S can be evaluated by Equation (3).

$$S_R = \frac{35.16504}{35} S \quad (3)$$

Combining the preceding equations and using the data of Table 1, Equation (4) is obtained, which determines the ionic strength of saline water only knowing its practical salinity (S).

$$I = \frac{19.9205352\, S}{1 - 1.004715429\, S} \quad (4)$$

Once these calculations were made, it was determined the most influential variables to focus on these variables for the generation of the Pourbaix diagrams. A variable was defined as influential if it can significantly modify the distribution of the stability areas in the diagrams. The selected variables were:

- Ions: cations (Ca^{2+}, K^+, Mg^{2+}, Na^+, Sr^{2+}) and anions (F^-, Br^-, CO_3^{2-}/HCO_3^-, Cl^-) were analyzed. Due to the software only accepts inputs of up to eight elements at the same time, being Cu the main. Firstly, each ion was analyzed separately along with copper, sulfur, and iron in the case of secondary and primary sulfides and then combined for each copper species and salinity concentrations. Only the anions CO_3^{2-}/HCO_3^-, Cl^- and Br^- affect the stability of the copper-solid species. Also, the concentration of CO_2 was analyzed for the salinity levels, but the stability diagrams do not change. The incidence of Boron was evaluated individually and together with the other ions for the three salinity levels, in all cases, no changes were observed in the stability diagrams. It is well known that CO_3^{2-}/HCO_3^- and $B(OH)_4^-/B(OH)_3$ ions are responsible for the alkaline pH of seawater, as well as its buffering capacity (Kochkodan et al., 2015). However, the latter does not generate copper complexes that can be seen in the diagrams. It is not possible to study $H_2CO_3/CO_3^{2-}/HCO_3^-$ or $B(OH)_4^-/B(OH)_3$ species separately because they are in equilibrium. The most important parameter, which determines a ratio of boric acid molecules to borate ions and carbonic acid, carbonate ion to bicarbonate ion in water, is the pH of the medium. The monovalent borate anion $B(OH)_4^-$ and CO_3^{2-} dominates at higher pH while non-ionized boric acid $B(OH)_3$ and H_2CO_3 at lower pH, HCO_3^- ion dominates at pH between 6 to 9. The distribution of boric acid and borate in seawater change moderately with salinity (Zeebe and Wolf-Gladrow, 2011).
- Copper concentration: Two copper concentrations were analyzed, 10^{-6} m and 1 m. The Pourbaix diagrams were constructed for all six copper-solid species with both concentrations. The results were opposite, finding small corrosion areas for the higher concentration and more prominent and clear areas for the lowest concentration. The copper concentration is a critical variable; thus, it was decided to use an intermedia concentration. An average copper concentration for the pregnant leach solution (PLS) of 0.07 m is used, this concentration is only referential, being able to use another one different in the range of 1^{-6} – 1 m.
- Temperature: Three temperatures were analyzed, 298 K, 323 K, and 353 K. The Pourbaix diagrams were constructed, and it was found a decrease in the corrosion areas when the temperature was increased for all copper-solid species.

Finally, the Pourbaix diagrams were constructed for six solid species (CuS, Cu_2S, CuO, Cu_2O, $CuFeS_2$, and Cu_5FeS_4). The seawaters considered the ions ($H_2CO_3/CO_3^{2-}/HCO_3^-$, Cl^- and Br^-), with the salinity levels (0, 35, 50, and 70‰) and their respective ionic strengths for pure water, seawater, brackish water, and brine, respectively. The copper concentration used was 0.07 mol/kg, and the temperature condition was 298 K. Once constructed the diagrams, the stability, corrosion, and passivation zones were subsequently analyzed. All the graphs are provided in appendix A, supplementary data.

3. Results and discussion

The Pourbaix diagrams were constructed using the reference composition of seawater, brackish water, and brine shown in Table 2.

Initially, the diagrams were produced for pure water and all oxides and sulfide copper species. The temperature considered is 298 K. As an example, in Fig. 1. shows the Pourbaix diagrams for CuO and Cu_2S. For all the solid species, the diagrams show the copper corrosion area for pH below 4 and potential up to 250 mV. Therefore, to ensure the transfer of Cu^{2+} ions into the leaching solution, the potential was increased, and pH decreased significantly.

Once the salinity is increased, complexation changes the corrosion areas for all the solid species. When the salinity is increased to 35‰, solid complexes appear, producing an increase in the total copper

Table 2. Reference Composition of seawater, brackish water and brine, and their respective ionic strengths

	Seawater	Brackish water	Brine
S (‰)	35	50	70
S_R (‰)	35.16504	50.23577	70.33008
I (mol/kg)	0.72263	1.04871	1.49993
Solute concentration, m_i (mol/kg)			
Na^+	0.48606	0.70539	1.00889
Mg^{2+}	0.05474	0.07944	0.11363
Ca^{2+}	0.01066	0.01547	0.02212
K^+	0.01058	0.01535	0.02196
Sr^{2+}	0.00009	0.00014	0.00020
Cl^-	0.56576	0.82106	1.17433
SO_4^{2-}	0.02926	0.04247	0.06074
HCO_3^-	0.00178	0.00258	0.00370
Br^-	0.00087	0.00127	0.00181
CO_3^{2-}	0.00025	0.00036	0.00051
$B(OH)_4^-$	0.00010	0.00015	0.00022
F^-	0.00007	0.00010	0.00015
OH^-	0.00001	0.00001	0.00002
$B(OH)_3$	0.00033	0.00047	0.00068
CO_2	0.00001	0.00001	0.00002

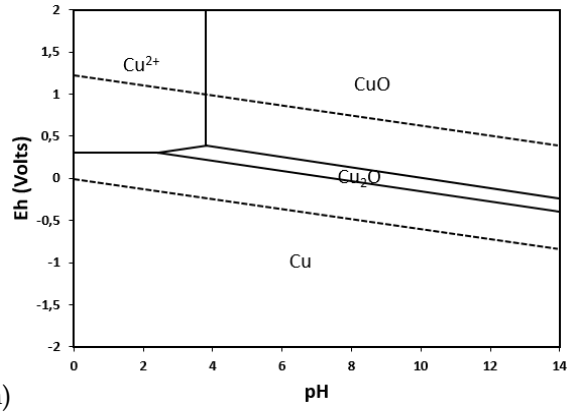

a)

$$Cu + 2H^+ \rightarrow Cu^{2+} + H_2$$

$$Cu^{2+} + H_2O \rightarrow CuO + 2H^+$$

$$2Cu + H_2O \rightarrow Cu_2O + H_2$$

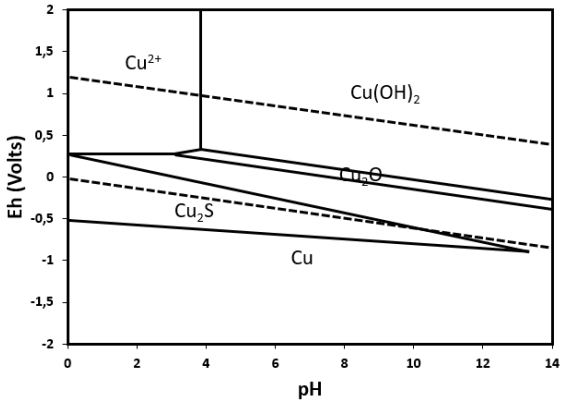

b)

$$Cu + 2H^+ \rightarrow Cu^{2+} + H_2$$

$$Cu^{2+} + 2H_2O \rightarrow Cu(OH)_2 + 2H^+$$

$$2Cu + H_2O \rightarrow Cu_2O + H_2$$

$$Cu_2S + 0.5O_2 + 2H^+ \rightarrow Cu^{2+} + S^0 + H_2O$$

Fig. 1. Pourbaix Diagrams for pure water 0 ‰ at 298 K and 0.07 m of Cu. a) Solid species CuO, b) Solid species Cu_2S

dissolution. The $CuCl_2 \cdot 3Cu(OH)_2$ and CuCl are formed, decreasing the corrosion area for all the solid species in the water stability zone (Fig. 2). The pH in the corrosion area remains below 4, but the potential increases close to 500 mV. The $CuCl_2 \cdot 3Cu(OH)_2$ formation consumes hydroxyl ions, which produces a decrease in the pH of the solution, desirable in the leaching stage. When the salinity increases to 50‰, $CuCl_3^{2-}$ is formed instead of CuCl, increasing the corrosion area to potentials less than 250 mV and pH 6, except for the Cu_5FeS_4 and $CuFeS_2$. The latter species have reduced $CuCl_3^{2-}$ area due to the formation of the solid species $Cu_2O \cdot Fe_2O_3$, as a result of iron contribution to the system. On the other hand, $Cu_2(OH)_2CO_3$ solid complex appears as a result of the increased concentration ion CO_3^{2-} and HCO_3^- ions (Fig. 3). The $Cu_2(OH)_2CO_3$ formation consumes CO_3^{2-} and HCO_3^- ions, which produces an even greater decrease in the pH of the solution.

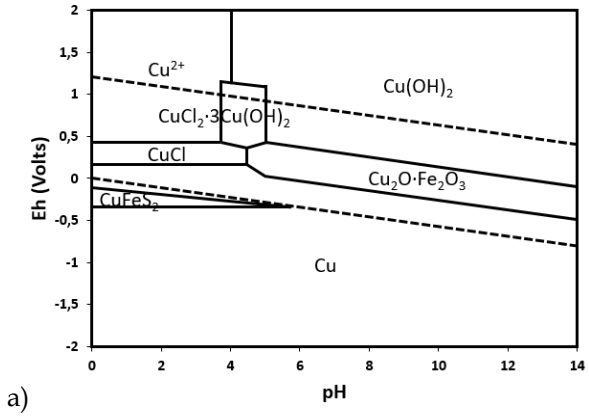

a)

$$CuFeS_2 + 4H^+ \rightarrow Cu^{2+} + Fe^{2+} + 2H_2S$$

$$Cu^{2+} + 2H_2O \rightarrow Cu(OH)_2 + 2H^+$$

$$2Cu + H_2O \rightarrow Cu_2O + H_2$$

$$Cu + Cl^- + H^+ \rightarrow CuCl + 0.5H_2$$

$$Cu^{2+} + 2Cl^- \rightarrow CuCl_2$$

$$Fe^{2+} + 0.25O_2 + 0.5H_2O \rightarrow Fe^{3+} + OH^-$$

$$2Fe^{3+} + 3H_2O \rightarrow Fe_2O_3 + 6H^+$$

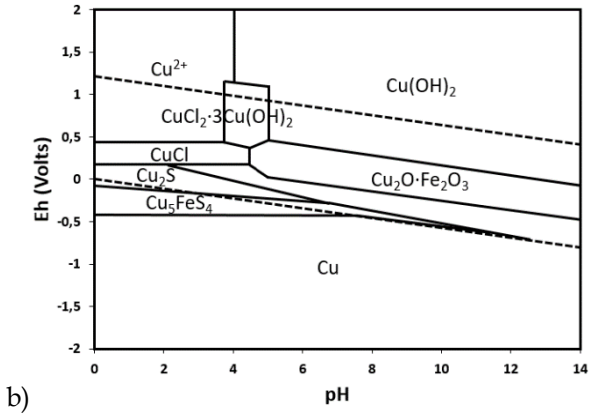

b)

$$Cu_5FeS_4 + 4H^+ + 9O_2 \rightarrow 5Cu^{2+} + Fe^{2+} + 4SO_4^{2-} + 2H_2O$$

$$Cu^{2+} + 2H_2O \rightarrow Cu(OH)_2 + 2H^+$$

$$2Cu + H_2O \rightarrow Cu_2O + H_2$$

$$Cu + Cl^- + H^+ \rightarrow CuCl + 0.5H_2$$

$$Cu^{2+} + 2Cl^- \rightarrow CuCl_2$$

$$Fe^{2+} + 0.25O_2 + 0.5H_2O \rightarrow Fe^{3+} + OH^-$$

$$2Fe^{3+} + 3H_2O \rightarrow Fe_2O_3 + 6H^+$$

$$4Cu_5FeS_4 \rightarrow 2Cu_2S + 4FeS + S_2$$

Fig. 2. Pourbaix Diagrams for seawater 35 ‰ at 298 K and 0.07 m of Cu, ions effect (Br-, CO_3^{2-}, Cl-). a) Solid species $CuFeS_2$, b) Solid Species Cu_5FeS_4

The vertical line between Cu^{2+} and $CuCl_2 \cdot 3Cu(OH)_2$ in Fig. 3 indicates that the reaction is independent of Eh, i.e., electrons do not take part in that reaction. On the other hand, the horizontal lines between Cu^{2+} and $CuCl_3^{2-}$ show that neither H^+ nor OH^- participate in these reactions but electrons take part.

In the last case, the increase of the salinity is to 70‰, a new area is found, the formation of the $CuCl^+$ complex, this corresponds to an oxidative corrosion area, which is overlap to the Cu^{2+} corrosion area. The increasing of the chlorine concentration contributes to the formation of $CuCl^+$ and increased $CuCl_3^{2-}$ area, increasing the corrosion area to potentials close to 0 mV and pH ranges higher than 6 in the water stability zone (Fig. 4). However, the formation of $CuCl^+$ may not be beneficial for the downstream stages due to the highly corrosive nature of this compound.

According to the representation obtained in Fig. 4, the use of seawater in hydrometallurgical processes of copper may result in the generation of copper compounds and chlorinated complexes, such as $CuCl_2 \cdot 3Cu(OH)_2$, CuCl, $Cu_2(OH)_2CO_3$, $CuCl_3^{2-}$ and $CuCl^+$. This observation was confirmed in the

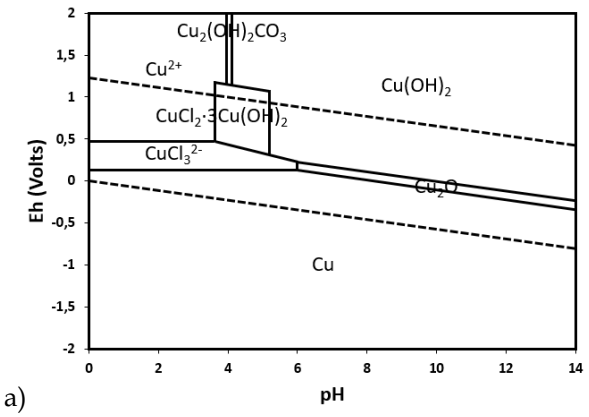

a)

$$Cu + 2H^+ \rightarrow Cu^{2+} + H_2$$

$$2Cu + H_2O \rightarrow Cu_2O + H_2$$

$$2Cu^{2+} + CO_3^{2-} + 2OH^- \rightarrow Cu_2(OH)_2CO_3$$

$$Cu^{2+} + 2H_2O \rightarrow Cu(OH)_2 + 2H^+$$

$$Cu^{2+} + 2Cl^- \rightarrow CuCl_2$$

$$Cu^+ + 3Cl^- \rightarrow CuCl_3^{2-}$$

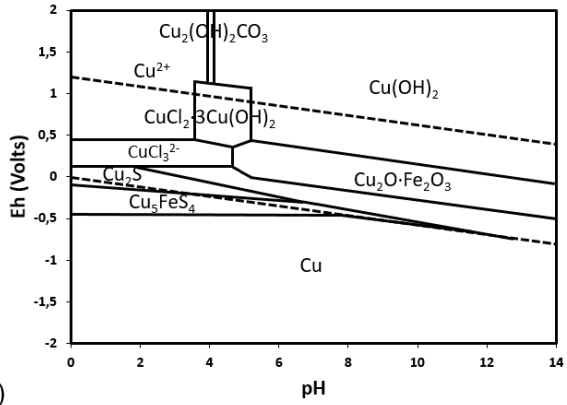

b)

$$Cu_5FeS_4 + 4H^+ + 9O_2 \rightarrow 5Cu^{2+} + Fe^{2+} + 4SO_4^{2-} + 2H_2O$$

$$2Cu^{2+} + CO_3^{2-} + 2OH^- \rightarrow Cu_2(OH)_2CO_3$$

$$Cu^{2+} + 2H_2O \rightarrow Cu(OH)_2 + 2H^+$$

$$2Cu + H_2O \rightarrow Cu_2O + H_2$$

$$Cu^{2+} + 2Cl^- \rightarrow CuCl_2$$

$$Cu^+ + 3Cl^- \rightarrow CuCl_3^{2-}$$

$$Fe^{2+} + 0.25O_2 + 0.5H_2O \rightarrow Fe^{3+} + OH^-$$

$$2Fe^{3+} + 3H_2O \rightarrow Fe_2O_3 + 6H^+$$

$$4Cu_5FeS_4 \rightarrow 2Cu_2S + 4FeS + S_2$$

Fig. 3. Pourbaix diagrams for brackish water 50 ‰ at 298 K and 0.07 m of Cu, ions effect (Br-, CO_3^{2-}, Cl^-). a) Solid species Cu_2O, b) Solid species Cu_5FeS_4

experiments developed by Hernández et al. (2015). They demonstrated that copper dissolution from chalcopyrite ($CuFeS_2$) using seawater is higher than using freshwater, through an increase in recoveries from 16 to 28%. Similarly, Torres et al. (2015) leached a low-grade fine-sized sulfide mineral (Cu_2S-$CuFeS_2$) using seawater, reaching extractions of 70-80%, which increase up to 90-97% when adding NaCl and Cu(II) as a catalyst. The result of these experiments can be attributed to the formation of complexes such as $CuCl^+$, which promotes the chemical reaction of dissolution. The horizontal lines between $CuCl^+$ and $CuCl_3^{2-}$ in Fig. 4 show that neither H^+ nor OH^- participate in these reactions but electrons take part. However, electrons and H^+/OH^- participate in the reaction between Cu^{2+} and $CuCl^+$.

If Pourbaix diagrams for the Cu_2O, CuO, Cu_2S, CuS in brine are compared with the pure water diagrams, it can be noted a significant increase in the total corrosion areas reaching pH values above 6 and potentials close to 0 mV due to the formation of the $CuCl_3^{2-}$ complex. The $CuCl_3^{2-}$ is well known in the leaching of sulfide ore, which leading the formation of a porous sulfide layer, increasing the copper diffusion through the ore. On the other hand, for the Cu_5FeS_4 and $CuFeS_2$, their corrosion areas reach pH close to 5 and potentials above 0 mV. In this case, the corrosion decreased due to the formation of the stable solid $Cu_2O{\cdot}Fe_2O_3$. This result can be significant in the flotation of chalcopyrite ore. The Eh-pH diagrams show that the copper and copper-iron sulfides turn to copper oxides and iron oxides, which likely form fast on the surface of the sulfides. Once the oxides are on the sulfide surfaces, these surfaces become more hydrophilic, more flotation collector is required to render them hydrophobic, and the mineral floatability lowers (Cruz et al., 2020). Copper oxides are more soluble than copper sulfides, so there will be more copper ions, which would cause un-wanted activation of pyrite and make more difficult the selective flotation of copper sulfides against pyrite as was observed by Mu and Peng (2019).

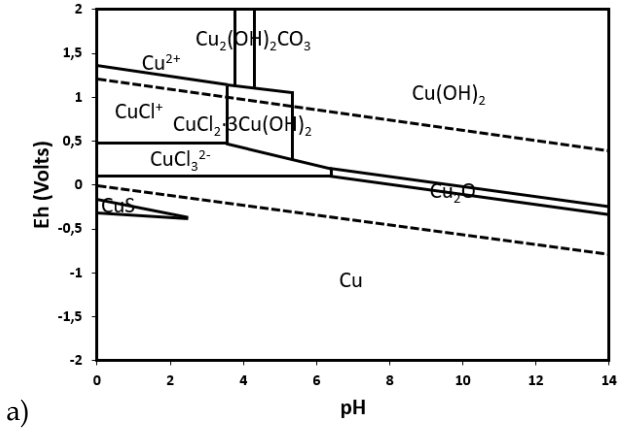

a)

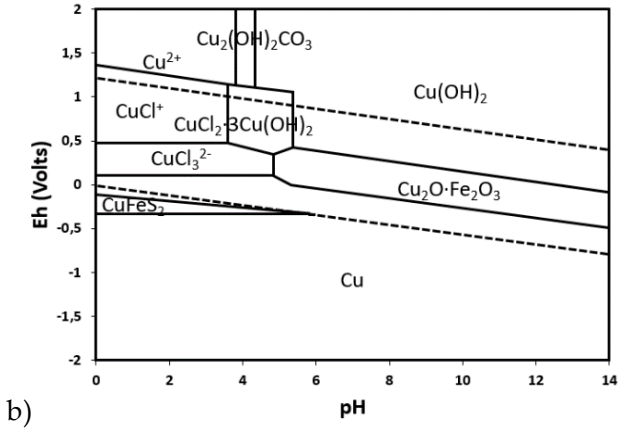

b)

$$Cu + 2H^+ \rightarrow Cu^{2+} + H_2$$

$$2Cu + H_2O \rightarrow Cu_2O + H_2$$

$$2Cu^{2+} + CO_3^{2-} + 2OH^- \rightarrow Cu_2(OH)_2CO_3$$

$$Cu^{2+} + 2H_2O \rightarrow Cu(OH)_2 + 2H^+$$

$$Cu^{2+} + 2Cl^- \rightarrow CuCl_2$$

$$Cu^{2+} + Cl^- \rightarrow CuCl^+$$

$$Cu^+ + 3Cl^- \rightarrow CuCl_3^{2-}$$

$$CuS + 2H^+ \rightarrow Cu^{2+} + H_2S$$

$$CuFeS_2 + 4H^+ \rightarrow Cu^{2+} + Fe^{2+} + 2H_2S$$

$$2Cu^{2+} + CO_3^{2-} + 2OH^- \rightarrow Cu_2(OH)_2CO_3$$

$$Cu^{2+} + 2H_2O \rightarrow Cu(OH)_2 + 2H^+$$

$$2Cu + H_2O \rightarrow Cu_2O + H_2$$

$$Cu^{2+} + Cl^- \rightarrow CuCl^+$$

$$Cu^{2+} + 2Cl^- \rightarrow CuCl_2$$

$$Cu^+ + 3Cl^- \rightarrow CuCl_3^{2-}$$

$$Fe^{2+} + 0.25O_2 + 0.5H_2O \rightarrow Fe^{3+} + OH^-$$

$$2Fe^{3+} + 3H_2O \rightarrow Fe_2O_3 + 6H^+$$

Fig. 4. Pourbaix Diagrams for brine 70‰ at 298 K and 0.07 m of Cu, ions effect (Br-, CO_3^{2-}, Cl-). a) Solid species CuS, b) Solid species $CuFeS_2$

The presence of different ions can visibly change the corrosion area. In the case of Cl^- and CO_3^{2-}, several species appear, $CuCl_2 \cdot 3Cu(OH)_2$ and CuCl for a salinity of 35‰, $Cu_2(OH)_2CO_3$ and $CuCl_3^{2-}$ for a salinity of 50‰, and $CuCl^+$ for a salinity of 70‰. The ion Br^- does not appear in any of the diagrams, but Br is present as CuBr. This occurs because the corrosion $CuCl_3^{-2}$ area is overlap on the CuBr area, due to the concentration of Cl^- is about 650 times greater than of Br^-. The concentration is not the unique variable that can change the corrosion area, but also temperature and pH. When the temperature increases, the activity of Cu(II) also increases, resulting in a diminution of the redox potential, and therefore, a decrease of its corrosion area. For this system, the potential also decreases with the increase of pH.

Finally, it is worth mentioning that the use of seawater in copper mining is nothing new; in northern Chile, several mining operations use it in their hydrometallurgical processes, as well as in their concentration processes via mineral flotation. The seawater has both favorable and harmful elements for metallurgical processes. Thus, it is relevant to define which interfering elements can be removed selectively, being possible to determine the suitable water quality for a specific metal that improves the performance of these processes. The choice of the best alternative, either seawater is used raw, partially desalinated, or desalinated, can be determined through the information obtained by Pourbaix diagrams. Moreover, partial or selective desalination is presented as a more viable alternative than total desalination, mainly due to the high energy cost of the latter. This will allow decreasing costs, greater efficiency in the process, and a lower impact on the environment (Herrera-León et al., 2019).

4. Conclusions

The Pourbaix diagram is a useful tool for the prediction of the thermodynamic stability area. The influence of the pH and potential on the formation of solid stable species and the passivation and corrosion areas can be analyzed.

The results obtained from Pourbaix diagrams for copper ores predict the formation of different species such as $CuCl_2 \cdot 3Cu(OH)_2$, CuCl, $Cu_2(OH)_2CO_3$, $CuCl_3^{2-}$ and $CuCl^+$, as the salinity of seawater increases. The generation of these species produces more extensive corrosion areas, which allows flexibility in the leaching operational variables, decreasing acid consumption and less oxidizing reagents. The increase in the corrosion areas starts from areas delimited for pH less than 4 and potentials above 250 mV for pure water to areas delimited for pH values above 6 and potentials close to 0 mV. The positive effect of this increase of corrosion areas is also observed in experiments performed by other authors, where the copper recoveries from sulfide ores are enhanced by using chlorinated solutions based on seawater.

Finally, the use of seawater, brackish water, and brine in mining processes is a more sustainable alternative instead of use freshwater, especially in locations with complex water availability, like northern Chile.

Acknowledgments

The authors are grateful for the support of the National Agency for Research and Development (ANID, Chile) through the Grant Proyecto Anillo ACM 170005. The authors also thank the Department of Chemical Engineering and Mineral Processes, Universidad de Antofagasta (Chile) for permanent support. O. Marin thanks ANID for a scholarship in support of national doctoral studies (Grant 21181949). The authors also thank to Alejandro López-Valdivieso for the discussion about flotation in seawater. O.M. thanks the Doctoral Program in Mineral Processing (Doctorado en Ingeniería de Procesos de Minerales) of the Universidad de Antofagasta.

Appendix A. Eh-pH Diagrams

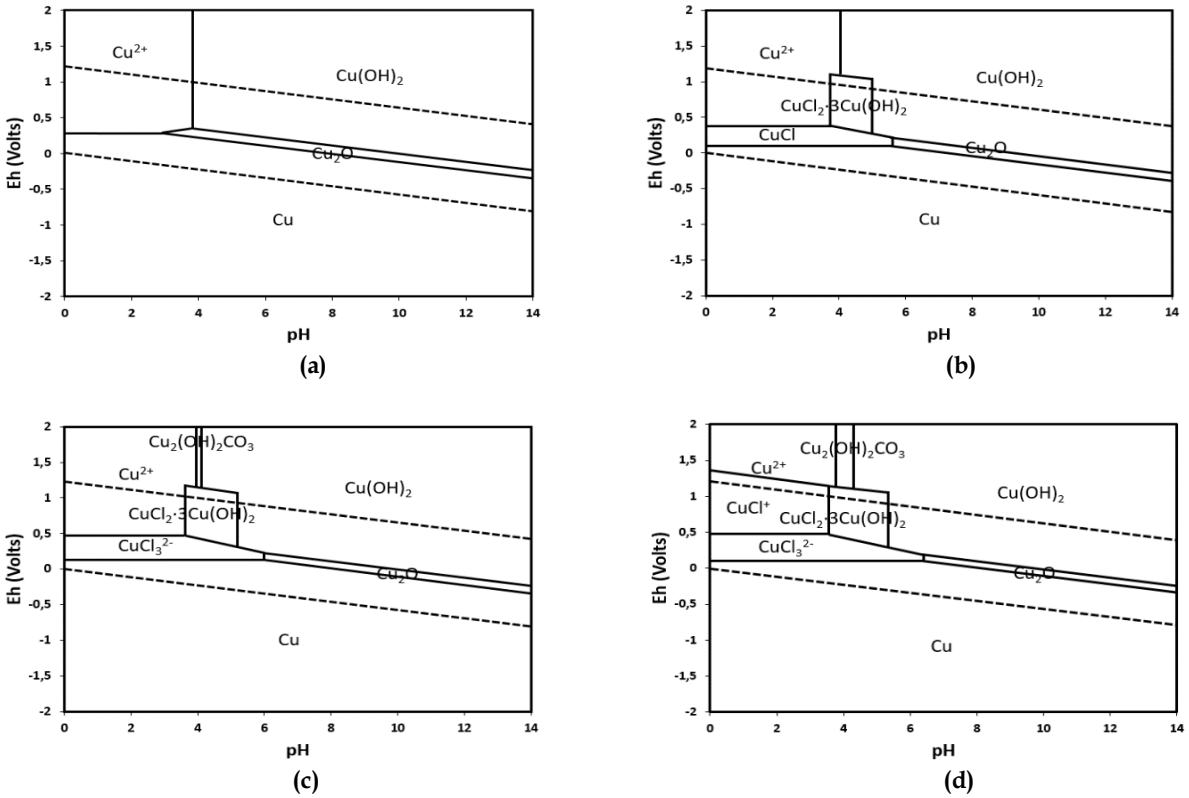

Fig. S1. Pourbaix Diagrams for Cu_2O at 25 °C and 0.07 m of Cu, ions effect (Br^-, CO_3^{-2}, Cl^-)
(a) Pure water (0 ‰); (b) Seawater (35 ‰); (c) Brackish water (50 ‰); (d) Brine (70 ‰)

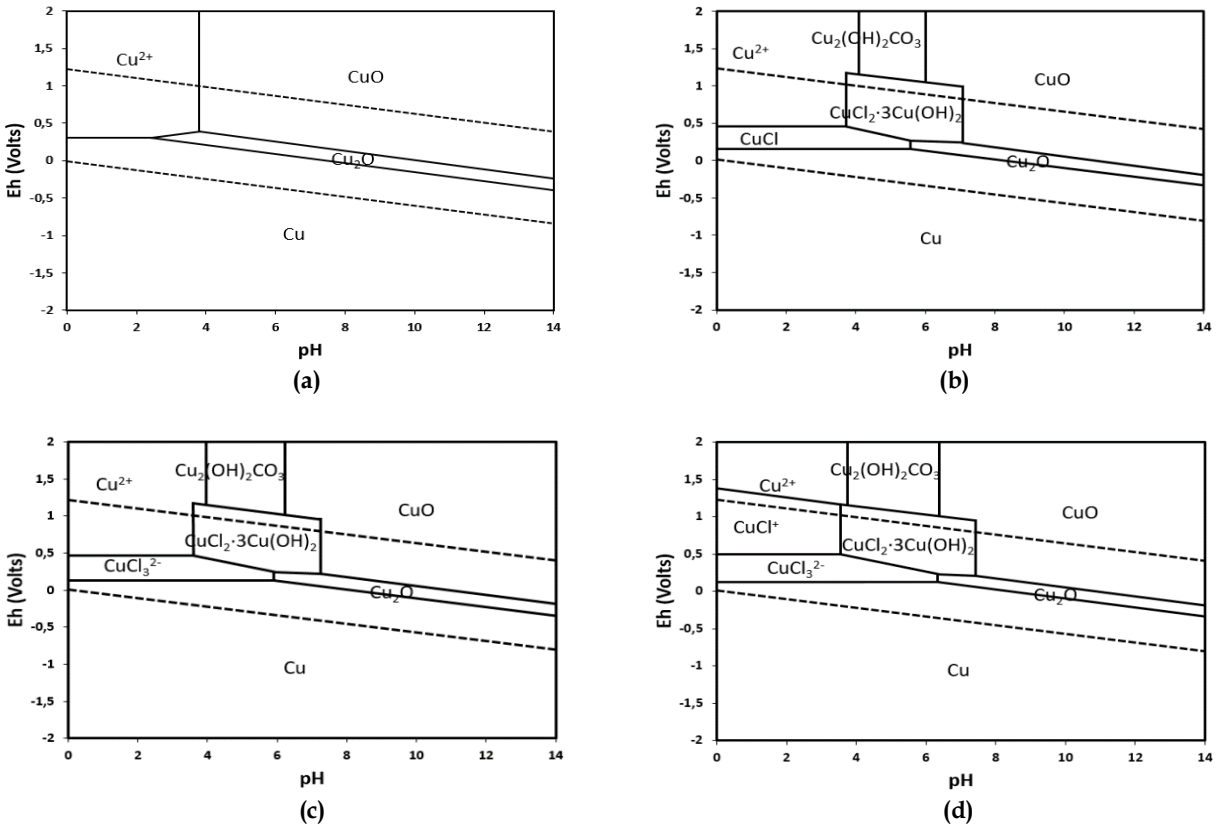

Fig. S2. Pourbaix Diagrams for CuO at 25 °C and 0.07 m of Cu, ions effect (Br^-, CO_3^{-2}, Cl^-)
(a) Pure water (0 ‰); (b) Seawater (35 ‰); (c) Brackish water (50 ‰); (d) Brine (70 ‰)

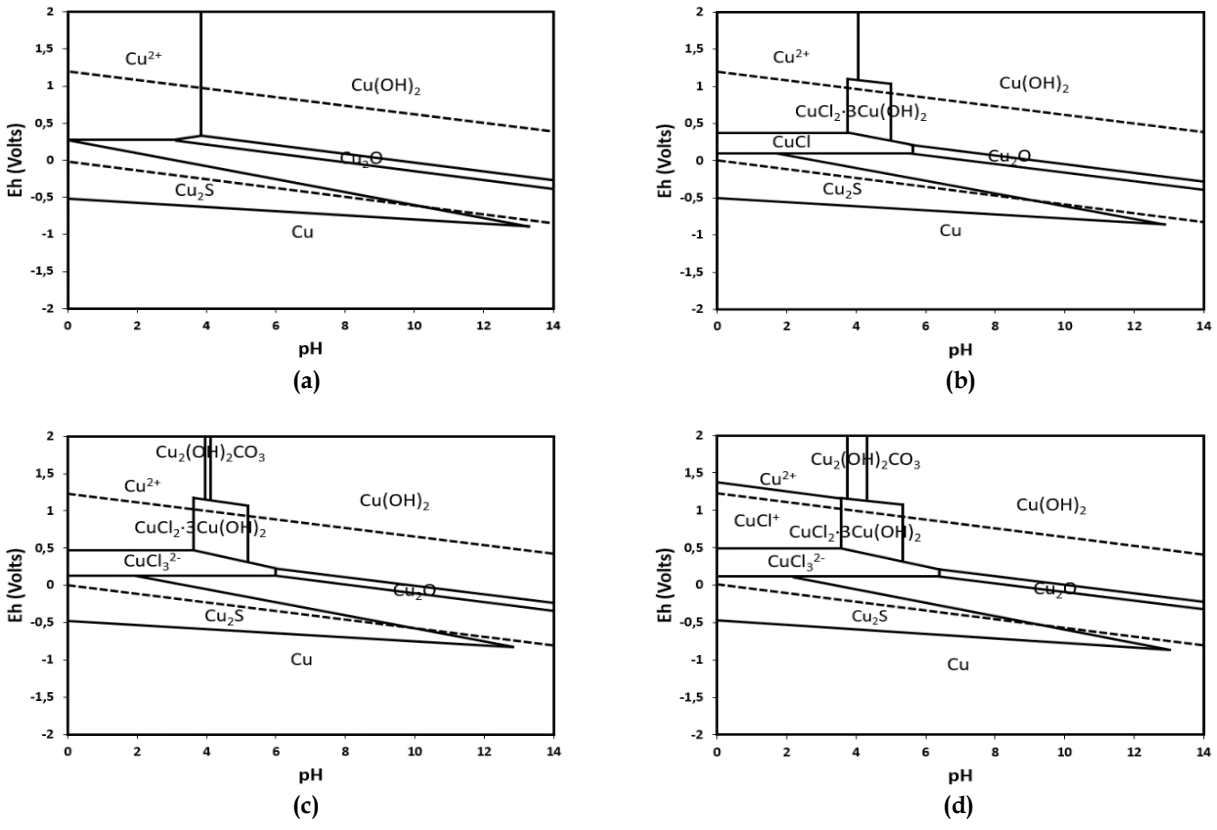

Fig. S3. Pourbaix Diagrams for Cu_2S at 25 °C and 0.07 m of Cu, ions effect (Br^-, CO_3^{-2}, Cl^-)
(a) Pure water (0 ‰); (b) Seawater (35 ‰); (c) Brackish water (50 ‰); (d) Brine (70 ‰)

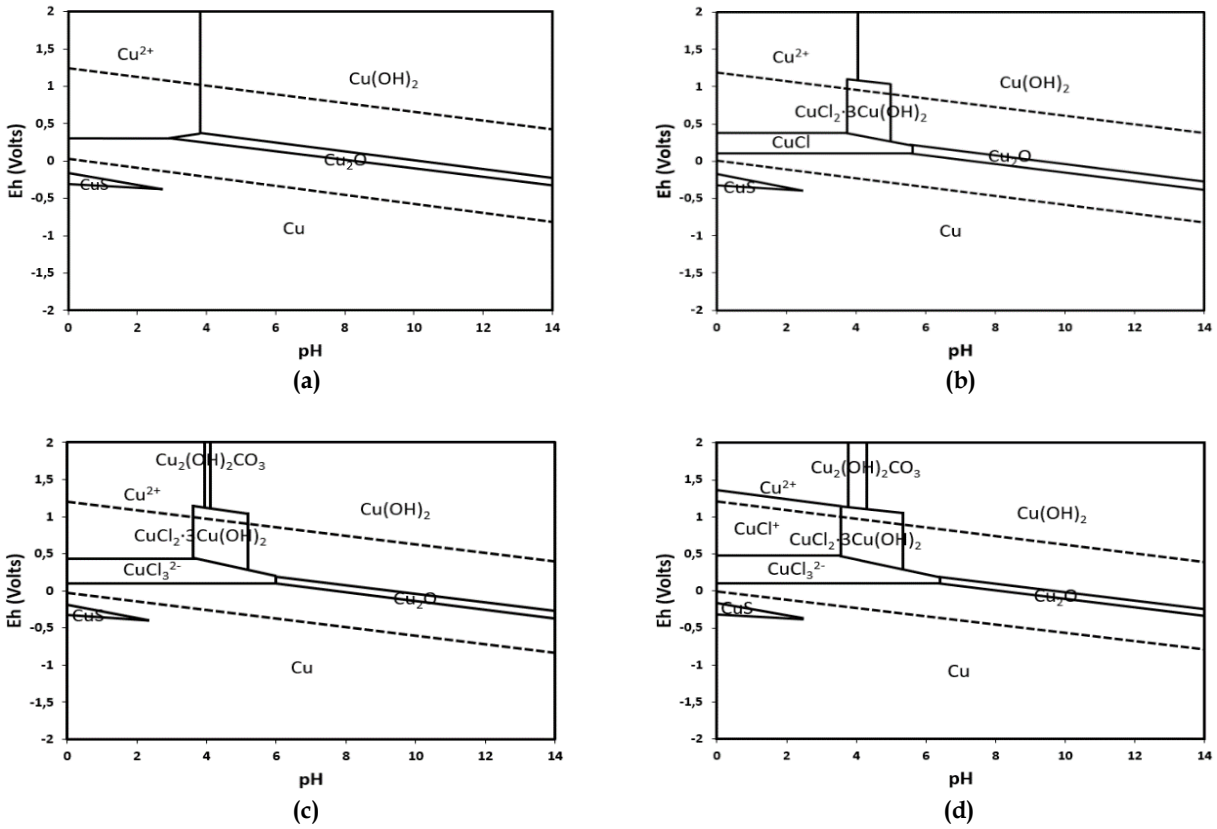

Fig. S4. Pourbaix Diagrams for CuS at 25 °C and 0.07 m of Cu, ions effect (Br^-, CO_3^{-2}, Cl^-)
(a) Pure water (0 ‰); (b) Seawater (35 ‰); (c) Brackish water (50 ‰); (d) Brine (70 ‰)

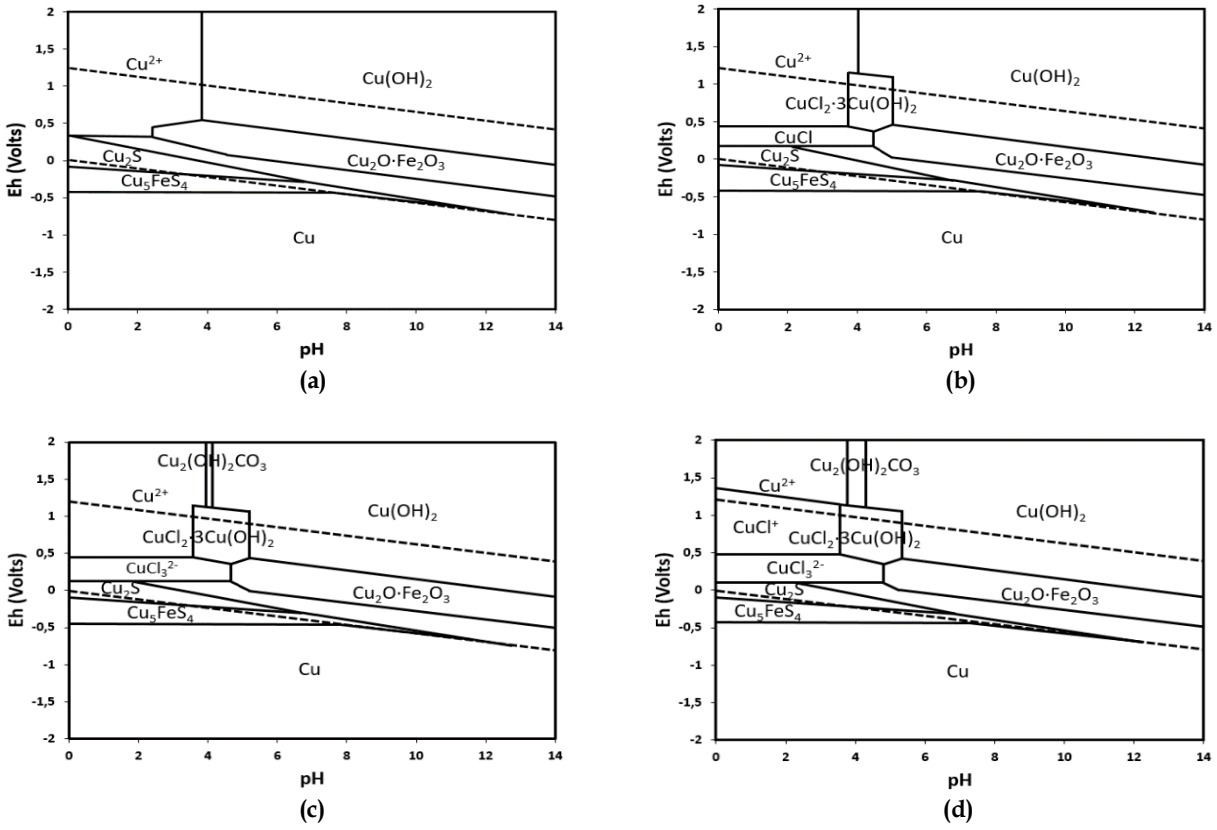

Fig. S5. Pourbaix Diagrams for Cu_5FeS_4 at 25 °C and 0.07 m of Cu, ions effect (Br^-, CO_3^{-2}, Cl^-)
(a) Pure water (0 ‰); (b) Seawater (35 ‰); (c) Brackish water (50 ‰); (d) Brine (70 ‰)

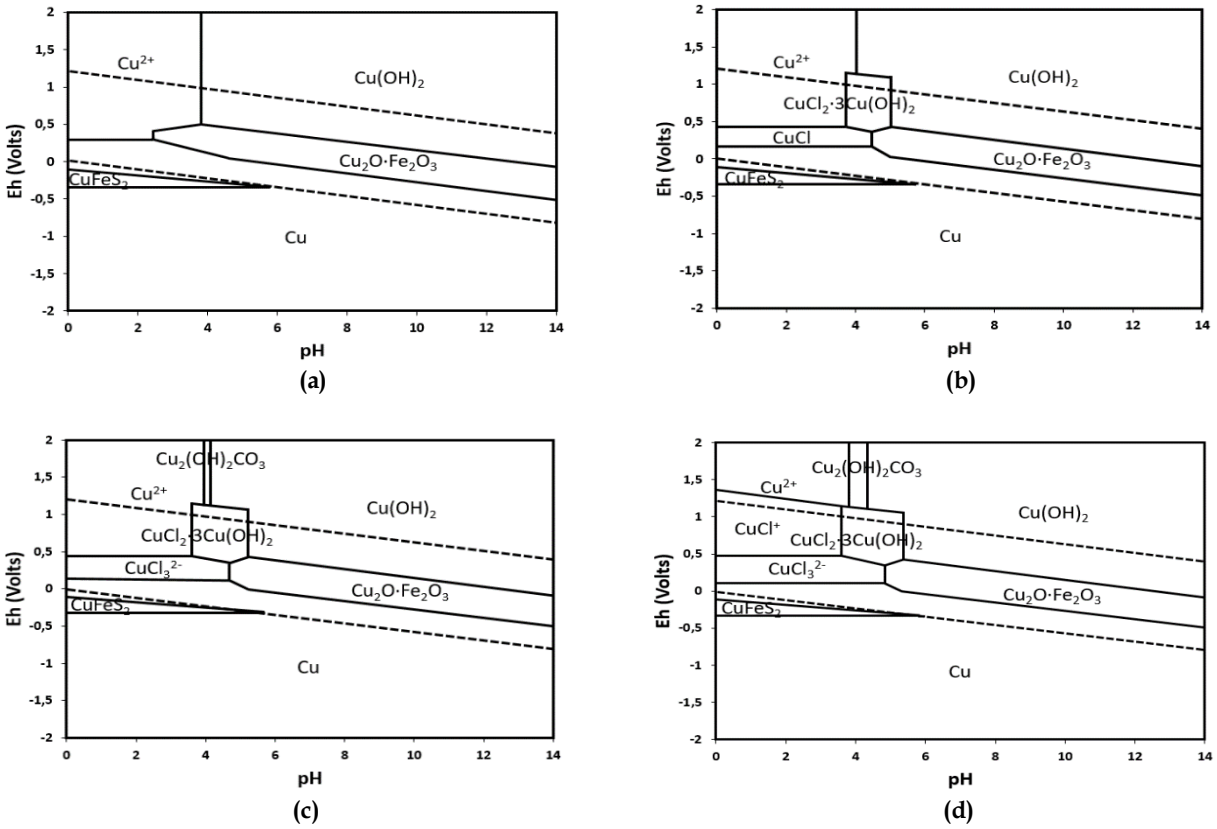

Fig. S6. Pourbaix Diagrams for $CuFeS_2$ at 25 °C and 0.07 m of Cu, ions effect (Br^-, CO_3^{-2}, Cl^-)
(a) Pure water (0 ‰); (b) Seawater (35 ‰); (c) Brackish water (50 ‰); (d) Brine (70 ‰)

References

ALI, Y., PRETAROLI, R., SOCCI, C., SEVERINI, F., 2018. *Carbon and water footprint accounts of Italy: A Multi-Region Input-Output approach.* Renew. Sustain. Energy Rev. 81, 1813–1824.

BELMONGE, M.R., MADRID, M.M., PEREZ-QUIROZ, J.T., SALAS, B.V., JUAREZ-ARELLANO, E.A., SCHORR, M., 2015. *Surface modification of carbon steel reinforcement of concrete*. Anti-Corrosion Methods Mater. 62, 69–76.

BYRND, R.H., 2002. *Inorganic speciation of dissolved elements in seawater: The influence of ph on concentration ratios. Inorg*. Chem. React. Struct. Mech. 3, 205–216.

BYRNE, R.H., KUMP, L.R., CANTRELL, K.J., 1988. *The influence of temperature and pH on trace metal speciation in seawater*. Mar. Chem. 25, 163–181.

CASTRO, S., 2018. *Physico-chemical factors in flotation of Cu-Mo-Fe ores with seawater: A critical review.* Physicochem. Probl. Miner. Process. 54, 1223–1236.

CAVIN, L., 2017. *Freshwater Environments and Fishes, in: Freshwater Fishes: 250 Million Years of Evolutionary History*. ISTE Press Ltd - Elsevier Ltd, pp. 1–14.

CISTERNAS, L.A., GALVEZ, E.D., 2017. *The use of seawater in mining. Miner. Process.* Extr. Metall. Rev. 1–16.

CISTERNAS, L.A., GALVEZ, E.D., 2014. *Chile's mining and chemicals industries*. Chem. Eng. Prog. 110, 46–51.

CLARKE, D., COSTA, D., ARBAB, F., 2006. *Connector Colouring I: Synchronisation and Context Dependency.* Electron. Notes Theor. Comput. Sci. 154, 101–119.

COCHILCO, 2019. *Anuario de Estadisticas del Cobre y Otros Minerales 1999-2018*. Com. Chil. del Cobre.

CRUZ, C., RAMOS, J., ROBLES, P., LEIVA, W.H., JELDRES, R.I., CISTERNAS, L.A., 2020. *Partial seawater desalination treatment for improving chalcopyrite floatability and tailing flocculation with clay content.* Miner. Eng. 151, 106307.

CRUZ, C., REYES, A., JELDRES, R.I., CISTERNAS, L.A., KRASLAWSKI, A., 2019. *Using Partial Desalination Treatment To Improve the Recovery of Copper and Molybdenum Minerals in the Chilean Mining Industry.* Ind. Eng. Chem. Res. 58, 8915–8922.

DEZFOOLIAN, M., RASHCHI, F., NEKOUEI, R.K., 2015. *Synthesis of copper and zinc oxides nanostructures by brass*

anodization in alkaline media. Surf. Coatings Technol. 275, 245–251.

DIXON, R.E., 2013. *Northern Chile and Peru: a hotspot for desalination*. Desalin. Water Treat. 51, 5–10.

ELIMELECH, M., PHILLIP, W.A., 2011. *The future of seawater desalination: Energy, technology, and the environment*. Science (80-.). 333, 712–717.

FAN, Y., YANG, Y., XIAO, Y., ZHAO, Z., LEI, Y., 2013. *Recovery of tellurium from high tellurium-bearing materials by alkaline pressure leaching process: Thermodynamic evaluation and experimental study*. Hydrometallurgy 139, 95–99.

GALVEZ, E.D., CISTERNAS, L.A., 2017. *Innovative Solutions for Seawater Use in Mining Operations*. Case Study Innov. Proj. - Success. Real Cases. https://doi.org/10.5772/intechopen.68191

HAUNG, H.-H., 2016. *The Eh-pH Diagram and Its Advances. Metals* (Basel). 6, 23.

HAUNG, H.-H., 1989. *Construction of Eh–pH and Other Stability Diagrams of Uranium in a Multicomponent System with a Microcomputer – II. Distribution Diagrams*. Can. Metall. Q. 28, 235–239.

HAUNG, H.-H., CUENTAS, L., 1989. *Construction of Eh–pH and Other Stability Diagrams of Uranium in a Multicomponent System with a Microcomputer – I. Domains of Predominance Diagrams*. Can. Metall. Q. 28, 225–234.

HERNANDEZ, P.C., TABOADA, M.E., HERREROS, O.O., GRABER, T.A., GHORBANI, Y., 2018. *Leaching of chalcopyrite in acidified nitrate using seawater-based media*. Minerals 8, 238.

HERNANDRZ, P.C., TABOADA, M.E., HERREROS, O.O., TORRES, C.M., GHORBANI, Y., 2015. *Chalcopyrite dissolution using seawater-based acidic media in the presence of oxidants*. Hydrometallurgy 157, 325–332.

HERRERA-LEON, S., CRUZ, C., KRASLAWSKI, A., CISTERNAS, L.A., 2019. Current situation and major challenges of desalination in Chile. Desalin. water Treat. 171, 93–104.

HOEKSTRA, A.Y., CHAPAGAIN, A.K., 2008. *Globalization of Water: Sharing the Planet's Freshwater Resources, Globalization of Water: Sharing the Planet's Freshwater Resources*. Blackwell Publishing Ltd.

JELDRES, R.I., FORBES, L., CISTERNAS, L.A., 2016. *Effect of Seawater on Sulfide Ore Flotation: A Review. Miner*. Process. Extr. Metall. Rev. 37, 369–384.

KOBYLIN, P., MAENPAA, L., ROINE, A., ANTTILA, K., 2014. *E-pH (Pourbaix) Diagrams Module*, in: HSC Chemistry 8.0. p. 16.

KOCHKODAN, V., DARWISH, N. BIN HILAL, N., 2015. *The Chemistry of Boron in Water*, in: Boron Separation Processes. Elsevier, pp. 35–63.

LAGOS, G., PETERS, D., VIDELA, A., JARA, J.J., 2018. *The effect of mine aging on the evolution of environmental footprint indicators in the Chilean copper mining industry 2001–2015*. J. Clean. Prod. 174, 389–400.

LOIZIDES, L., 2000. T*he Cost of Environmental and Social Sustainability of Desalination* . Source: <http://gwri-ic.technion.ac.il/pdf/IDS/96.pdf>.

LUO, T., YOUND, R., REIG, P., 2015. A*queduct projected water stress country rankings*. Technical Note. Washington D.C.

MILLER, G., 1998. *Factors controlling heap leaching performance with fine and clayey ores*, in: ALTA 1998. Perth, Australia, p. 24.

MILLERO, F., WOOSLEY, R., DITROLIO, B., WATERS, J., 2009. *Effect of Ocean Acidification on the Speciation of Metals in Seawater*. Oceanography 22, 72–85.

MILLERO, F.J., 1974. *The Physical Chemistry of Seawater*. Annu. Rev. Earth Planet. Sci. 2, 101–150.

MILLERO, F.J., FEISTEL, R., WRIGHT, D.G., MCDOUGALL, T.J., 2008. *The composition of Standard Seawater and the definition of the Reference-Composition Salinity Scale*. Deep. Res. Part I Oceanogr. Res. Pap. 55, 50–72.

MU, Y., PENG, Y., 2019. *The effect of saline water on copper activation of pyrite in chalcopyrite flotation*. Miner. Eng. 131, 336–341.

NORTHEY, S., HAQUE, N., MUDD, G., 2013. *Using sustainability reporting to assess the environmental footprint of copper mining*. J. Clean. Prod. 40, 118–128.

NORTHEY, S.A., MUDD, G.M., SAARIVUORI, E., WESSMAN-JAASKELAINEN, H., HAQUE, N., 2016. *Water footprinting and mining: Where are the limitations and opportunities*? J. Clean. Prod. 135, 1098–1116.

ORDONEZ, J.I., KORENO, L., GONZALEZ, J.F., CISTERNAS, L.A., 2015. *Use of discharged brine from reverse osmosis plant in heap leaching: Opportunity for caliche mining industry*. Hydrometallurgy 155, 61–68.

POURBAIX, M., 1966. *Atlas of electrochemical equilibria in aqueous solutions*. Pergamon Press, New York.

SU, G., GAO, X., DU, L., ZHANG, D., HU, J., LIU, Z., 2016. *Influence of Mn on the corrosion behaviour of medium manganese steels in a simulated seawater environment*. Int. J. Electrochem. Sci. 11, 9447–9461.

SUYANTARA, G.P.W., HIRAJIMA, T., MIKI, H., SASAKI, K., 2018. *Floatability of molybdenite and chalcopyrite in artificial seawater*. Miner. Eng. 115, 117–130.

TORRES, C.M., TABOADA, M.E., GRABER, T.A., HERREROS, O.O., GHORBANI, Y., WATLING, H.R., 2015. *The effect of seawater based media on copper dissolution from low-grade copper ore*. Miner. Eng. 71, 139–145.

VALDERRAMA, J.O., CAMPUSANO, R.A., GALVEZ, E.D., 2017. *Correlation and Prediction of the Solubility of Air Gases in Saline Solutions for Mining Processes, Using Artificial Neural Networks*. Clean - Soil, Air, Water 45, 1500902. https://doi.org/10.1002/clen.201500902

VELASQUEZ-YEVENES, L., QUEZADA-REYES, V., 2018. *Influence of seawater and discard brine on the dissolution of copper ore and copper concentrate*. Hydrometallurgy 180, 88–95.

VON BONSDORFF, R., JARVENPAA, N., AROMAA, J., FORSEN, O., HYVARINEN, O., BARKER, M.H., 2005. *Electrochemical sensors for the HydroCopper™ process solution*. Hydrometallurgy 77, 155–161.

WANG, B., PENG, Y., 2014. *The effect of saline water on mineral flotation - A critical review*. Miner. Eng. 66, 13–24.

WANG, H., WEN, S., HAN, G., FENG, Q., 2019. *Effect of copper ions on surface properties of ZnSO4-depressed sphalerite and its response to flotation*. Sep. Purif. Technol. 228.

WATLIN, H.R., 2014. *Chalcopyrite hydrometallurgy at atmospheric pressure: 2. Review of acidic chloride process options*. Hydrometallurgy 146, 96–110.

WRIGHT, J., COLLING, A., 1995. *Seawater: its Composition, Properties and Behaviour*. Elsevier.

XING, P, MA, B., WANG, C., CHEN, Y., 2019. *Extraction and separation of zinc, lead, silver, and bismuth from bismuth slag*. Physicochem. Probl. Miner. Process. 55, 173–183.

YAGI, S., NAKANISHI, H., ICHITSUBO, T., MATSUBARA, E., 2009. *Oxidation-State Control of Nanoparticles Synthesized via Chemical Reduction Using Potential Diagrams*. J. Electrochem. Soc. 156, D321.

YANG, B., ZENG, Z., WANG, X., YIN, X., CHEN, S., 2014. *Pourbaix diagrams to decipher precipitation conditions of Si-Fe-Mn-oxyhydroxides at the PACMANUS hydrothermal field*. Acta Oceanol. Sin. 33, 58–66.

YEPSEN, R., GUTIERREZ, L., LASKOWSKI, J., 2019. *Flotation behavior of enargite in the process of flotation using seawater*. Miner. Eng. 142, 105897.

ZEEBE, R.E.; WOLF-GLADROW, D., 2011. *CO2 in Seawater: Equilibrium, Kinetics, Isotopes*. Elsevier Science.